

## Single-particle dynamics of the Anderson model: a two-self-energy description within the numerical renormalization group approach

This article has been downloaded from IOPscience. Please scroll down to see the full text article.

2005 J. Phys.: Condens. Matter 17 6959

(<http://iopscience.iop.org/0953-8984/17/43/013>)

View [the table of contents for this issue](#), or go to the [journal homepage](#) for more

Download details:

IP Address: 129.252.86.83

The article was downloaded on 28/05/2010 at 06:36

Please note that [terms and conditions apply](#).

# Single-particle dynamics of the Anderson model: a two-self-energy description within the numerical renormalization group approach

Martin R Galpin and David E Logan

Physical and Theoretical Chemistry Laboratory, University of Oxford, South Parks Road, Oxford OX1 3QZ, UK

Received 11 July 2005, in final form 23 August 2005

Published 14 October 2005

Online at [stacks.iop.org/JPhysCM/17/6959](http://stacks.iop.org/JPhysCM/17/6959)

## Abstract

Single-particle dynamics of the Anderson impurity model are studied using both the numerical renormalization group (NRG) method and the local moment approach (LMA). It is shown that a ‘two-self-energy’ description of dynamics inherent to the LMA, as well as a conventional ‘single-self-energy’ description, arise within NRG; each yielding correctly the same local single-particle spectrum. Explicit NRG results are obtained for the broken symmetry spectral constituents arising in a two-self-energy description, and the total spectrum. These are also compared to analytical results obtained from the LMA as implemented in practice. Very good agreement between the two is found, essentially on all relevant energy scales from the high-energy Hubbard satellites to the low-energy Kondo resonance.

## 1. Introduction

The numerical renormalization group (NRG) method [1, 2] forms a well established, powerful numerical technique for calculating the properties of quantum impurity and related models. The basic paradigm here is of course the celebrated Anderson impurity model (AIM) [3], in particular the Kondo effect arising in strong coupling (see [4] for a review). NRG is not restricted to calculation of static properties, but can equally handle dynamical properties such as single-particle spectra, see e.g. [5–7].

Dynamics in particular pose well known difficulties for analytical approaches [4]; be it in handling strong correlations in general, spanning the full relevant range of energy scales, satisfying the low-energy dictates of Fermi liquid behaviour and so on. In recent years we have been developing a local moment approach (LMA) to single-particle dynamics and related properties of a range of quantum impurity models, see e.g. [8–14]. Physically transparent, and technically straightforward in practice, the LMA is based on an underlying ‘two-self-energy’ description. As in Anderson’s original work [3], local moments are introduced explicitly from the outset, leading to *two* degenerate mean-field saddle points. Spin-flip tunnelling between the

mean-field states—embodied in dynamical contributions to the two associated self-energies, naturally absent at pure mean-field level—lifts the erstwhile spin degeneracy of the saddle points, and restores the singlet symmetry characteristic of the local Fermi liquid state.

As implemented in practice the LMA is of course approximate, as dictated by the particular approximation chosen for the dynamical contributions to the two self-energies [8–13]. But it is taken for granted that, in principle, dynamics may be obtained either within an underlying two-self-energy framework, or within the ‘single-self-energy’ description that provides the conventional route to single-particle dynamics. In this case, it is natural to ask whether a two-self-energy description also arises within an essentially exact numerical approach such as NRG. It is this issue we consider here. We show that according to whether even or odd RG iterations are considered, both the single- and the two-self-energy descriptions are contained in the NRG approach, and in particular we obtain explicit NRG results for the composite broken symmetry spectra inherent to a TSE description. This in turn enables direct comparison to be made between NRG results for the underlying spectra and those arising from the LMA as implemented in practice. Very good agreement is found, on all energy scales characteristic of the problem. Results are given in section 3, following a brief discussion of the background theory in section 2.

## 2. Theory

The AIM Hamiltonian [3] is given in standard notation by

$$\hat{H} = \sum_{\mathbf{k},\sigma} \epsilon_{\mathbf{k}} \hat{n}_{\mathbf{k}\sigma} + \sum_{\sigma} \left( \epsilon_i + \frac{U}{2} \hat{n}_{i-\sigma} \right) \hat{n}_{i\sigma} + \sum_{\mathbf{k},\sigma} V_{i\mathbf{k}} (c_{i\sigma}^{\dagger} c_{\mathbf{k}\sigma} + \text{h.c.}) \quad (2.1)$$

where the first term refers to the non-interacting host, and the second to the impurity with local interaction  $U$  and energy  $\epsilon_i$ . In strong coupling (large  $U$ ) the low-energy physics of the AIM is of course that of the Kondo model [4]. Our focus is the  $T = 0$  local impurity spectrum  $D(\omega) = -\frac{1}{\pi} \text{Im} G(\omega)$ , with  $G(\omega) (\leftrightarrow G(t) = -i\theta(t)\langle\{c_{i\sigma}(t), c_{i\sigma}^{\dagger}\}\rangle)$  the impurity propagator,

$$G(\omega) = \frac{1}{[g^{-1}(\omega) - \Sigma(\omega)]}. \quad (2.2)$$

Here  $g(\omega) = [\omega^+ - \epsilon_i - \Delta(\omega)]^{-1}$  is the non-interacting propagator with  $\Delta(\omega) = \sum_{\mathbf{k}} V_{i\mathbf{k}}^2 [\omega^+ - \epsilon_{\mathbf{k}}]^{-1}$  the hybridization function, such that  $\Delta(\omega) = -i\Delta_0$  for a wide flat-band host [4], with  $\Delta_0 = \pi V^2 \rho_{\text{host}}(\omega = 0)$  the hybridization strength ( $\omega = 0$  refers to the Fermi level, and  $V \equiv V_{i\mathbf{k}}$ ).  $\Sigma(\omega) = \Sigma^R(\omega) - i\Sigma^I(\omega)$  denotes the interaction self-energy, which is merely defined by the Dyson equation implicit in equation (2.2).

It is of course  $\Sigma(\omega)$  that provides the conventional theoretical route to dynamics, via perturbation theory (PT) in  $U$  [4]. This approach is fine in principle, order by order in PT. But it is limited in practice, reflecting the inability of PT to handle strong correlations in general [4]. The practical difficulties arise because construction of  $\Sigma(\omega)$  via conventional PT based on Hartree-modified propagators, beginning with the static Hartree bubble diagram  $\Sigma^0$ , amounts to an expansion about the Hartree mean-field saddle point. And this single-determinantal saddle point is generally unstable to local moment condensation [3], reflected e.g. in the fact that the standard diagrammatic resummations one might expect to be required to capture strong correlations—such as the sum of all particle–hole interactions in the transverse spin channel—give rise to well known divergences/non-analyticities in  $\Sigma(\omega)$  [4, 8, 9].

In these circumstances the LMA simply recognizes [8–10] that the natural mean-field saddle point about which to expand is unrestricted Hartree–Fock, corresponding to condensed

local moments. Since  $\hat{H}$  is invariant under  $\sigma \leftrightarrow -\sigma$ , this saddle point is now of course doubly degenerate, denoted by  $\alpha = A$  or  $B$ , corresponding respectively to local moments  $\mu = +|\mu|$  and  $-|\mu|$ . Accordingly, the full  $G(\omega)$  is expressed as [8–10]

$$G(\omega) = \frac{1}{2}[G_{A\sigma}(\omega) + G_{B\sigma}(\omega)] \quad (2.3a)$$

$$= \left\{ \frac{1}{[g^{-1}(\omega) - \tilde{\Sigma}_{A\sigma}(\omega)]} + \frac{1}{[g^{-1}(\omega) - \tilde{\Sigma}_{B\sigma}(\omega)]} \right\} \quad (2.3b)$$

with self-energies  $\tilde{\Sigma}_{\alpha\sigma}(\omega) (= \tilde{\Sigma}_{\alpha\sigma}^0 + \Sigma_{\alpha\sigma}(\omega))$  with  $\tilde{\Sigma}_{\alpha\sigma}^0$  the static Hartree–Fock bubble). Note that equation (2.3a) is rotationally invariant, since the invariance of  $\hat{H}$  under  $\sigma \leftrightarrow -\sigma$  implies generally that  $G_{A\sigma}(\omega) = G_{B-\sigma}(\omega)$  and hence that  $G(\omega)$  is correctly independent of spin  $\sigma$ . Direct comparison of equations (2.2) and (2.3b) also clearly implies a general relation (equation (3.4) of [9]) between the single self-energy  $\Sigma(\omega)$  and the  $\{\tilde{\Sigma}_{\alpha\sigma}(\omega)\}$ , enabling the former to be obtained directly from the latter.

At this stage we emphasize the generality of the above considerations. The impurity propagator  $G(\omega)$ , and hence spectrum  $D(\omega)$ , may be obtained either via the conventional single-self-energy description embodied in equation (2.2), or via the two-self-energy (TSE) description inherent in equation (2.3): which one uses is a matter of choice, at least in principle. In practice, of course, the stability of the underlying mean-field (MF) saddle point arguably renders the TSE description a more natural choice. The standard diagrammatic resummations for the dynamical contribution  $\Sigma_{\alpha\sigma}(\omega)$  to  $\tilde{\Sigma}_{\alpha\sigma}(\omega)$  no longer suffer from non-analyticities, and as detailed in [8–10] may be employed with impunity. This forms the practical basis of the LMA. Moreover the relation mentioned above between  $\Sigma(\omega)$  and  $\{\tilde{\Sigma}_{\alpha\sigma}(\omega)\}$  may be employed to ascertain directly, and generally, the conditions on  $\{\tilde{\Sigma}_{\alpha\sigma}(\omega)\}$  under which  $\Sigma^I(\omega) \sim \mathcal{O}(\omega^2)$  as  $\omega \rightarrow 0$ , i.e. exhibits Fermi liquid behaviour. This is merely a matter of algebra, and as detailed in [9] the requisite condition is

$$\tilde{\Sigma}_{A\sigma}^R(0) = \tilde{\Sigma}_{B\sigma}^R(0) \quad (\equiv \Sigma^R(0)) \quad (2.4)$$

referring exclusively to the Fermi level  $\omega = 0$ . In an exact theory for the metallic AIM, this ‘symmetry restoration’ condition should be satisfied automatically (see also section 3). For the LMA in practice [8–10] it is enforced self-consistently, and thereby determines the local moment magnitude  $|\mu|$  (supplanting the usual gap equation for  $|\mu|$  at pure MF level) [8–10]. It is also central in being able to access the quantum phase transition to a degenerate local moment phase where such arises, as it does in the pseudogap AIM [12–15].

How well the LMA in practice captures single-particle dynamics can of course be tested by direct comparison to NRG calculations. For the metallic AIM, this has been considered in [10] (see also [14]). The resultant LMA scaling spectrum  $D(\omega)$  versus  $\omega/\omega_K$  in the strong coupling, Kondo regime was shown to be in excellent agreement with NRG results. However an issue evidently remains. Within the LMA the single-particle spectrum is expressed (equation (2.3)) as  $D(\omega) = \frac{1}{2}[D_{A\sigma}(\omega) + D_{B\sigma}(\omega)]$  (where  $D_{\alpha\sigma}(\omega) = -\frac{1}{\pi} \text{Im} G_{\alpha\sigma}(\omega)$ ). It is this that has hitherto been compared to NRG results. The considerations above suggest however that there should exist an NRG counterpart of the spectral densities  $D_{A\sigma}(\omega)$  and  $D_{B\sigma}(\omega)$  inherent to a TSE description. It is this we now consider. The resultant  $D_{\alpha\sigma}(\omega)$  can in turn be individually interrogated and compared to the detailed predictions for them arising from the LMA in practice.

### 2.1. NRG spectra

In Wilson’s NRG method [1, 2] the AIM is mapped onto a semi-infinite chain. This is diagonalized iteratively starting from the free impurity, and with a suitably truncated basis

such that with increasing chain length essentially only the lowest lying states are renormalized. Spectral functions at each iteration  $N$  are calculated [5, 6] from the appropriate matrix elements connecting the NRG ground state and excited states, themselves related recursively to those of the previous iteration; and the spectrum for the whole frequency range is built up from the results for all iterations (roughly speaking, iteration  $N$  determines the spectrum at frequencies  $\omega \sim D\Lambda^{-(N-1)/2}$  with  $D$  the conduction electron bandwidth and  $\Lambda$  the usual NRG discretization parameter [1, 2]). The resultant spectrum consists of a set of  $\delta$ -functions with known weights at discrete frequencies, which is then broadened on a logarithmic scale to recover the continuum, see specifically equation (10) of [7]. This is the standard approach to calculating  $T = 0$  spectra via the NRG, and we follow it here. (An alternative method [7] focuses directly on obtaining the self-energy  $\Sigma(\omega)$ . Although not used here, we simply remark that it can also be extended to encompass the TSE spectral description considered below.)

NRG spectra may be calculated from either the even set or the odd set of iterations (the fixed point, here exclusively strong coupling, is a fixed point of the square of the RG transformation [1, 2]). The same spectrum  $D(\omega)$  results in either case, as shown explicitly below. There is however an important difference between even- $N$  and odd- $N$  iterations. In the former case, the NRG ground state is always a non-degenerate spin singlet. For the odd- $N$  iterations by contrast we find that the NRG ground state (for any iteration) is a degenerate doublet,  $S = \frac{1}{2}$  (where we emphasize that  $S$  denotes the *total* spin angular momentum quantum number of the entire system). Denoting the  $S_z = +\frac{1}{2}$  component of this doublet by ‘A’, and the  $S_z = -\frac{1}{2}$  component by ‘B’, we can thus construct separate single-particle spectra (for either spin  $\sigma$ ) from each of these degenerate ground states, denoted by  $D_{A\sigma}(\omega)$  and  $D_{B\sigma}(\omega)$  respectively, such that the total, normalized single-particle spectrum is given simply by  $D(\omega) = \frac{1}{2}[D_{A\sigma}(\omega) + D_{B\sigma}(\omega)]$ . From the invariance of  $\hat{H}$  under  $\sigma \leftrightarrow -\sigma$  it follows that  $D_{A\sigma}(\omega) = D_{B-\sigma}(\omega)$ , whence only (say)  $D_{A\uparrow}(\omega)$  and  $D_{B\uparrow}(\omega)$  need be considered in general. And for the particle-hole symmetric AIM ( $\epsilon_i = -\frac{U}{2}$ ) considered explicitly below, it follows further that  $D_{\alpha\sigma}(\omega) = D_{\alpha-\sigma}(-\omega)$  ( $\alpha = A$  or  $B$ ), such that  $D_{B\uparrow}(\omega) = D_{A\downarrow}(\omega) = D_{A\uparrow}(-\omega)$  and  $D(\omega) = D(-\omega)$ .

The essential point of the preceding discussion is clear. NRG spectra arising from odd- $N$  iterations generate in effect a TSE description of single-particle dynamics, enabling both the  $D_{\alpha\sigma}(\omega)$  and the total spectrum  $D(\omega)$  to be determined. The even- $N$  NRG spectrum by contrast, arising as it does from the non-degenerate NRG ground state in this case, corresponds to a conventional single-self-energy description of dynamics, from which  $D(\omega)$  itself may again be obtained directly.

### 3. Results: NRG and LMA

To illustrate the above, figure 1 shows the resultant odd- $N$  NRG spectrum  $D_{A\uparrow}(\omega)$  versus  $\omega/\Delta_0$ , for the symmetric AIM with a strong coupling interaction strength  $\tilde{U} = U/\pi\Delta_0 = 12$  (calculated with  $\Lambda = 2$ , retaining  $\sim 10\,000$  states per iteration). We consider first the insets, which show the corresponding total spectrum  $D(\omega) = \frac{1}{2}[D_{A\uparrow}(\omega) + D_{B\uparrow}(\omega)]$  from the odd- $N$  iterations (solid line), as well as  $D(\omega)$  obtained from the even- $N$  iterations (dotted line). The resultant symmetric spectra consist as expected of two high-energy Hubbard satellites, symmetrically disposed at  $\omega \sim \pm\frac{U}{2}$ , and the low-energy Kondo resonance. The first fact to note is that the  $D(\omega)$  obtained from odd and even iterations are indistinguishable. This underscores the point made in section 2: in an essentially exact approach, such as NRG, the two-self-energy and single-self-energy descriptions are fundamentally equivalent, and which one employs is a matter of choice. We also add (see section 2) that the symmetry restoration

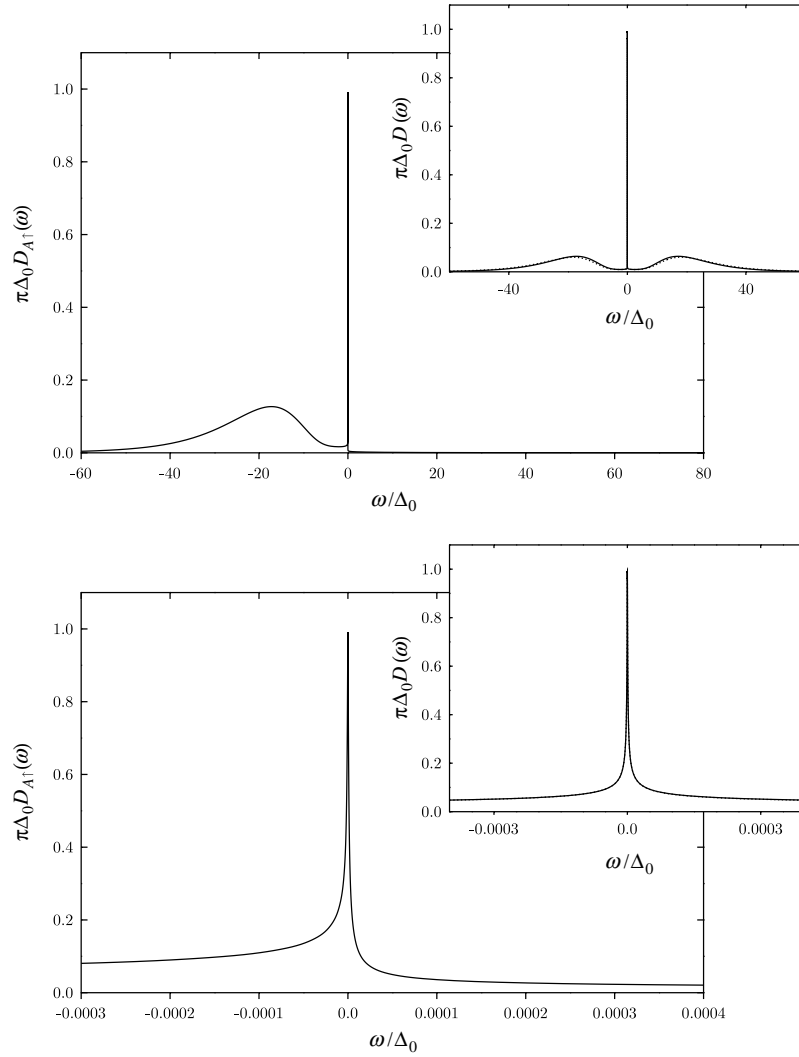


**Figure 1.** NRG spectrum  $\pi \Delta_0 D_{A\uparrow}(\omega)$  versus  $\omega/\Delta_0$  for  $\tilde{U} = 12$ . The upper panel shows  $D_{A\uparrow}(\omega)$  on ‘all scales’ including the single, high-energy Hubbard satellite and the Kondo resonance. The lower panel focuses on the asymmetric, low-energy Kondo resonance. Insets: the corresponding total spectrum  $D(\omega) = \frac{1}{2}[D_{A\uparrow}(\omega) + D_{B\uparrow}(\omega)] (=D(-\omega))$  obtained from the odd- $N$  iterations (solid line), and  $D(\omega)$  obtained from the even- $N$  iterations (dotted line); the two are in fact indistinguishable.

condition equation (2.4),  $\tilde{\Sigma}_{A\sigma}^R(0) = \tilde{\Sigma}_{B\sigma}^R(0)$  ( $=0$  for the symmetric AIM), is as expected satisfied within NRG, reflected in the fact that  $\pi \Delta_0 D_{A\uparrow}(\omega = 0) = \pi \Delta_0 D_{A\downarrow}(\omega = 0) = 1$  (as required by the Friedel sum rule/Luttinger integral theorem [4], and satisfied in practice to  $\lesssim 1\%$  accuracy in the present calculations).

Turning now to the main panels in figure 1, the obvious feature is the intrinsic asymmetry in  $D_{A\uparrow}(\omega)$ . Only a lower Hubbard satellite is seen in  $D_{A\uparrow}(\omega)$  (the upper satellite correspondingly arises in  $D_{B\uparrow}(\omega) = D_{A\uparrow}(-\omega)$ ); consistent with the expectation that the ‘A’ state ( $S_z = +\frac{1}{2}$ ) connects in the atomic limit ( $V_{ik} = 0$ ) to a purely  $\uparrow$ -spin occupied impurity, from which an

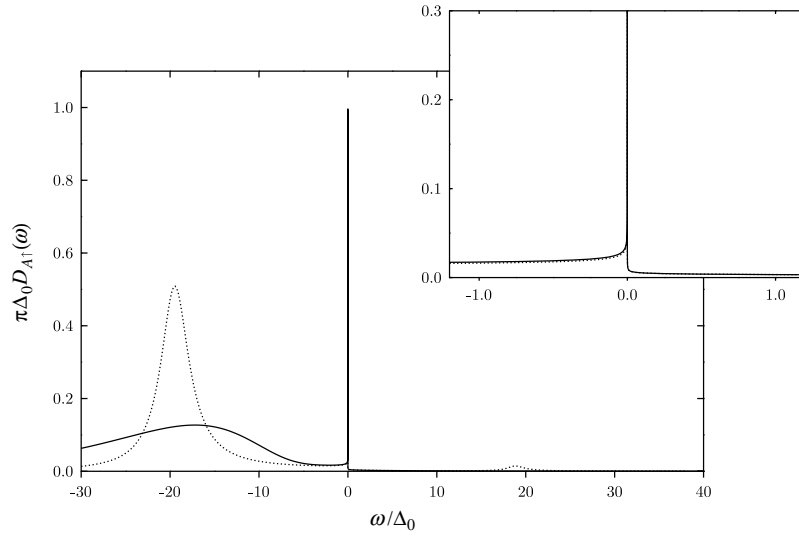


**Figure 2.**  $\pi \Delta_0 D_{A\uparrow}(\omega)$  versus  $\omega/\Delta_0$  for  $\tilde{U} = 12$ , obtained from NRG (solid line) and LMA (dotted line). The inset continues the comparison on a lower energy scale. NRG is known to overbroaden the high energy Hubbard satellite; this is reconstructed in figure 6, where further comparison is made between NRG and LMA.

$\uparrow$ -spin electron may be removed but not added. The asymmetry in  $D_{A\uparrow}(\omega)$  is not moreover confined to the high-energy spectrum highlighted in the upper panel, which has an obvious counterpart in the atomic limit: the low-energy Kondo resonance (lower main panel) is likewise seen to be strongly asymmetric.

To gain further insight into these results we now consider direct comparison with the LMA in practice, which affords an analytical handle on the single-particle dynamics. Full details of the underlying calculations are given in [8] for the symmetric AIM considered here (and in [9] for the asymmetric case). Here we focus purely on results arising.

In figure 2 NRG and LMA results for  $\pi \Delta_0 D_{A\uparrow}(\omega)$  are compared, versus  $\omega/\Delta_0$  (i.e. on an ‘absolute’ energy scale). The chosen  $\tilde{U} = 12$  is simply representative of the large  $\tilde{U}$ , strong coupling behaviour of interest; similar results to those that follow have naturally been obtained for a range of interaction strengths. Let us first comment on the lower Hubbard satellite in  $D_{A\uparrow}(\omega)$  (main panel), which clearly contains the vast majority of the spectral weight. The LMA satellite is itself a Lorentzian, with an HWHM of  $2\Delta_0$ —twice that occurring in the pure mean-field limit (for the physical reasons explained in [8]), and which behaviour is believed to be asymptotically exact in strong coupling. With NRG by contrast the Hubbard satellite is well known to be overbroadened, due to the associated broadening on a logarithmic scale [5, 6] (as occurs also, although ameliorated somewhat, with the method introduced in [7]). We will return to this below (see figure 6), and show that the NRG results for the satellite are in fact consistent with the above Lorentzian behaviour.

Aside from the high energy satellite issue, NRG and LMA results are seen from figure 2 to be in remarkably good agreement. That this persists down to much lower energy scales is shown further in figure 3, where  $D_{A\uparrow}(\omega)$  is shown in the top panel and the full symmetric spectrum  $D(\omega)$  in the lower panel. Our aim now is to obtain a handle on the characteristic asymmetry evident in the  $D_{A\uparrow}(\omega)$  Kondo resonance. This may be obtained analytically from the LMA [10], formally for  $|\tilde{\omega}| \gg 1$  where  $\tilde{\omega} = \omega/\omega_K$  and the Kondo scale  $\omega_K$  is (here

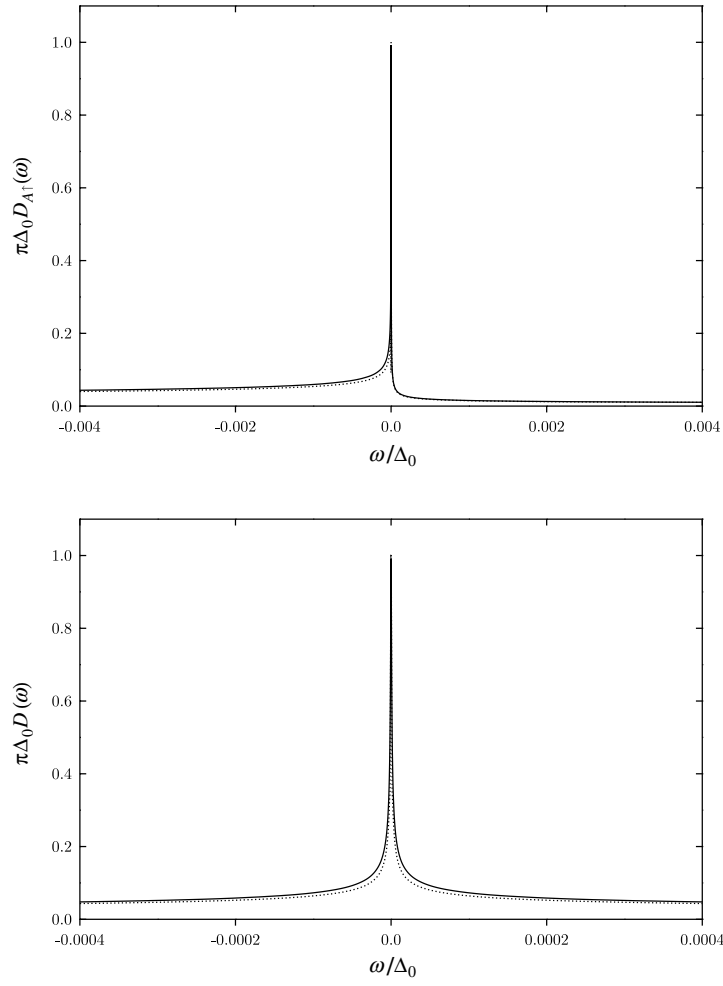


**Figure 3.** For  $\tilde{U} = 12$ , comparison between NRG (solid lines) and LMA (dotted lines) on the lowest energy scales appropriate to the Kondo resonance. Upper panel:  $\pi \Delta_0 D_{A\uparrow}(\omega)$  versus  $\omega/\Delta_0$ . Lower panel: the full spectrum  $\pi \Delta_0 D(\omega)$  versus  $\omega/\Delta_0$ , with  $D(\omega) = \frac{1}{2}[D_{A\uparrow}(\omega) + D_{B\uparrow}(\omega)]$ .

defined as) the HWHM of the Kondo resonance in  $D(\omega)$ . On the positive frequency side, for  $\tilde{\omega} = |\tilde{\omega}| \gg 1$ , the LMA gives the asymptotic behaviour [10]

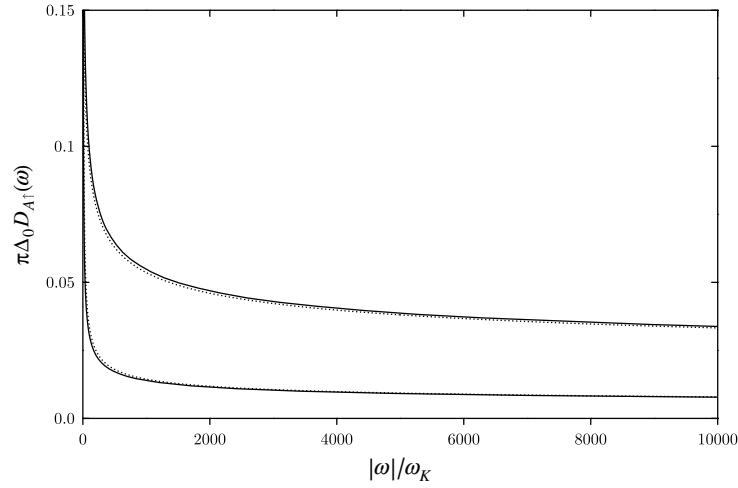
$$\pi \Delta_0 D_{A\uparrow}(\omega) = \frac{1}{\left[\frac{4}{\pi} \ln(a|\tilde{\omega}|)\right]^2 + 1} \quad (3.1)$$

with  $a \simeq 0.7$  a pure constant; while for negative frequencies by contrast, and  $-\tilde{\omega} = |\tilde{\omega}| \gg 1$ ,

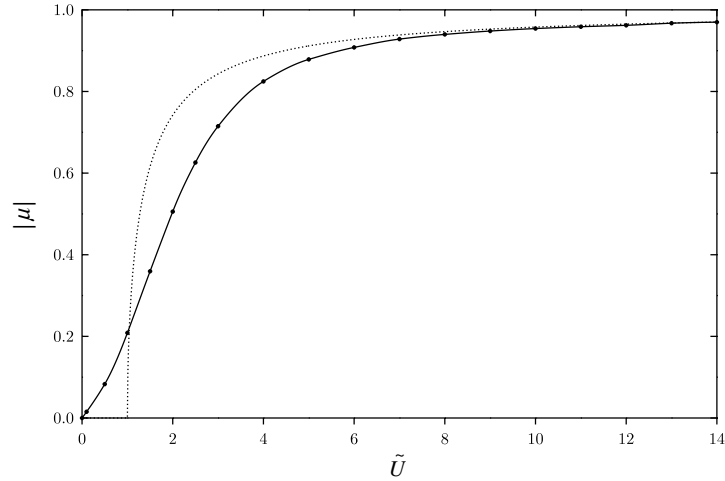
$$\pi \Delta_0 D_{A\uparrow}(\omega) = \frac{5}{\left[\frac{4}{\pi} \ln(a|\tilde{\omega}|)\right]^2 + 25}. \quad (3.2)$$

Figure 4 compares NRG results for  $\pi \Delta_0 D_{A\uparrow}(\omega)$  with this predicted asymptotic behaviour. The agreement is seen to be very good, and in practice equations (3.1) and (3.2) already describe the spectra quite accurately for  $|\omega|/\omega_K \gtrsim 2$  or so. We also add that the full forms of equations (3.1) and (3.2) are required for the agreement shown in figure 4, i.e. the





**Figure 4.** Comparison between NRG results for  $\pi \Delta_0 D_{A\uparrow}(\omega)$  versus  $|\omega|/\omega_K$  (solid lines) and the predicted asymptotic behaviour equations (3.1) and (3.2) (dotted lines). Lower curves, for positive frequencies,  $\omega > 0$ ; upper curves, for  $\omega < 0$ .



**Figure 5.** NRG local moment  $|\mu| = \int_{-\infty}^0 d\omega [D_{A\uparrow}(\omega) - D_{A\downarrow}(\omega)]$  versus  $\tilde{U} = U/\pi \Delta_0$  (solid line), compared to its mean-field counterpart (dotted line) which in strong coupling  $\tilde{U} \gg 1$  gives  $|\mu| \sim 1 - 4/\pi^2 \tilde{U}$ . The latter result is in fact asymptotically exact, and is seen to be recovered by NRG.

behaviour in the  $|\omega|/\omega_K$ -range shown is not dominated by the ultimate high frequency asymptotic behaviours of  $\pi^2/[16 \ln^2(|\omega|/\omega_K)]$  and  $5\pi^2/[16 \ln^2(|\omega|/\omega_K)]$ . For the full spectrum  $D(\omega) = \frac{1}{2}[D_{A\uparrow}(\omega) + D_{B\uparrow}(\omega)] \equiv \frac{1}{2}[D_{A\uparrow}(\omega) + D_{A\uparrow}(-\omega)]$  the corresponding result is obviously just the weighted sum of equations (3.1) and (3.2) (with ultimate asymptotic behaviour of  $3\pi^2/[16 \ln^2(|\omega|/\omega_K)]$  that is exact for the  $s = \frac{1}{2}$  Kondo model [10]). It has been shown in [10] that this result for  $D(\omega)$  itself is in excellent agreement with NRG results. We regard it as remarkable that the LMA provides an equally compelling description of the asymmetric  $D_{\alpha\sigma}(\omega)$ .

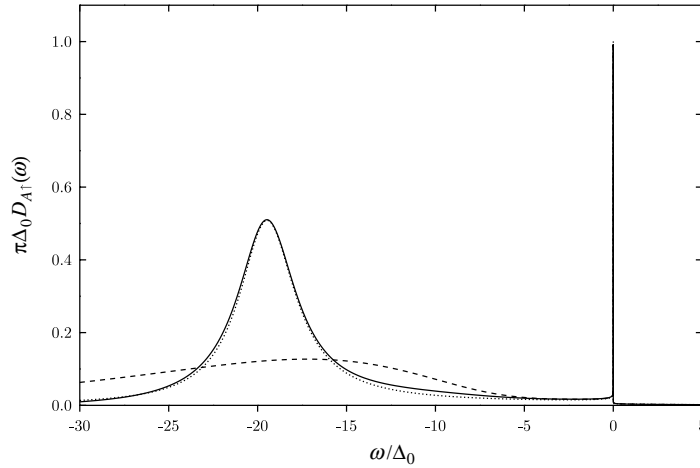


**Figure 6.**  $\pi \Delta_0 D_{A\uparrow}(\omega)$  versus  $\omega/\Delta_0$  for  $\tilde{U} = 12$  obtained from the LMA (dotted line) and NRG (solid line), with the NRG Hubbard satellite obtained as described in the text. The agreement is now excellent on all energy scales. The original, overbroadened NRG spectrum is shown for comparison (dashed line).

The fact that the  $D_{\alpha\sigma}(\omega)$  are strongly asymmetric also means of course that the degenerate odd- $N$  NRG ground states ‘A’ and ‘B’ carry a local moment, equal and opposite for the two states, with magnitude given by  $|\mu| = \int_{-\infty}^0 d\omega [D_{A\uparrow}(\omega) - D_{A\downarrow}(\omega)]$ . The resultant  $|\mu|$  is shown in figure 5 as a function of  $\tilde{U}$ , and compared to its pure mean-field counterpart. The latter is given from solution of<sup>1</sup>  $|\mu| = \frac{2}{\pi} \tan^{-1}(\frac{U|\mu|}{2\Delta_0})$  (and in practice the LMA  $|\mu|$  determined from symmetry restoration is very close to the MF value, exponentially so in strong coupling  $\tilde{U} \gg 1$  [8]). Recognizing that in strong coupling the Kondo resonance carries exponentially small weight and thus makes essentially no contribution to the resultant  $|\mu|$ , the leading asymptotic behaviour of the moment may be determined exactly from second order perturbation theory in the hybridization  $V_{ik}$ . It is found thereby to be given by  $|\mu| \sim 1 - 4/\pi^2 \tilde{U}$ , which amusingly is precisely the leading result obtained from pure mean-field, and which as seen from figure 5 is indeed recovered correctly from the NRG calculations.

We return finally to the issue of the overbroadened NRG Hubbard satellite, and show that the ‘raw’ NRG results are entirely consistent with a Lorentzian satellite of width  $2\Delta_0$ . To that end we calculate, as a sum of poleweights, the cumulative NRG spectrum  $F_{\text{NRG}}(\omega) = \int_{-\infty}^{\omega} d\omega' D_{A\uparrow}(\omega')$ ; the corresponding result for the pure Lorentzian would be  $F_L = \frac{1}{\pi} \tan^{-1}(\frac{\omega - \omega_0}{2\Delta_0}) + \frac{1}{2}$  with  $\omega_0 \sim -\frac{U}{2}$  the satellite maximum. Writing  $F_{\text{NRG}}(\omega) = F_L(\omega) + \delta F(\omega)$  with  $\delta F(\omega)$  thus defined, the NRG poles in  $D_{A\uparrow}(\omega)$  contributing to  $\delta F(\omega)$  are broadened in the usual logarithmic fashion, and added to the pure Lorentzian contribution (the net spectral weight below the Fermi level is of course preserved). If the NRG results are consistent with the Lorentzian, little deviation from this form should result. That this is indeed the case is shown in figure 6, and NRG and LMA results now agree well on all energy scales including the high-energy Hubbard satellite.

<sup>1</sup> We consider explicitly the usual ‘wide band’ case where the conduction bandwidth  $D$  is by far the largest energy scale.

#### 4. Concluding remarks

In this paper we have considered first a general issue: does a two-self-energy description of dynamics that is inherent to the local moment approach also arise within the numerical renormalization group method? The answer to this question is clearly yes—both it and a conventional single-self-energy framework arise naturally within NRG, according to whether odd or even RG iterations are considered. In consequence, explicit NRG results for the composite broken symmetry spectra underlying the two-self-energy description may be obtained:  $D_{A\sigma}(\omega)$  and  $D_{B\sigma}(\omega)$  such that  $D(\omega) = \frac{1}{2}[D_{A\sigma}(\omega) + D_{B\sigma}(\omega)]$  gives the total impurity spectrum (and with  $D(\omega)$  coincident for both odd/even iterations). These in turn have been compared to results arising from the LMA as it is implemented in practice, and very good agreement found on essentially all characteristic energy scales from the high-energy Hubbard satellites to the low-energy Kondo resonance.

We also add that our essential conclusion is naturally not specific to the metallic Anderson impurity model considered here: a two-self-energy description will arise for essentially any quantum impurity model, such as the pseudogap AIM [12, 14–16] (where the TSE description is in general a necessity and not a luxury), and more generally for lattice-based models such as the periodic Anderson model within the framework of dynamical mean-field theory [16].

#### Acknowledgment

We are grateful to the EPSRC for supporting this research.

#### References

- [1] Wilson K G 1975 *Rev. Mod. Phys.* **47** 773
- [2] Krishnamurthy H R, Wilkins J W and Wilson K G 1980 *Phys. Rev. B* **21** 1003  
Krishnamurthy H R, Wilkins J W and Wilson K G 1980 *Phys. Rev. B* **21** 1044
- [3] Anderson P W 1961 *Phys. Rev.* **124** 41
- [4] Hewson A C 1993 *The Kondo Problem to Heavy Fermions* (Cambridge: Cambridge University Press)
- [5] Sakai O, Shimizu Y and Kasuya T 1989 *J. Phys. Soc. Japan* **58** 3666
- [6] Costi T A, Hewson A C and Zlatić V 1994 *J. Phys.: Condens. Matter* **6** 2519
- [7] Bulla R, Pruschke T and Hewson A C 1998 *J. Phys.: Condens. Matter* **10** 8365
- [8] Logan D E, Eastwood M P and Tusch M A 1998 *J. Phys.: Condens. Matter* **10** 2673
- [9] Glossop M T and Logan D E 2002 *J. Phys.: Condens. Matter* **14** 6737
- [10] Dickens N L and Logan D E 2001 *J. Phys.: Condens. Matter* **13** 4505
- [11] Logan D E and Dickens N L 2002 *J. Phys.: Condens. Matter* **14** 3605
- [12] Logan D E and Glossop M T 2000 *J. Phys.: Condens. Matter* **12** 985
- [13] Glossop M T and Logan D E 2003 *J. Phys.: Condens. Matter* **15** 7519
- [14] Bulla R, Glossop M T, Logan D E and Pruschke T 2000 *J. Phys.: Condens. Matter* **12** 4899
- [15] Withoff D and Fradkin E 1990 *Phys. Rev. Lett.* **64** 1835
- [16] Smith V E, Logan D E and Krishnamurthy H R 2003 *Eur. Phys. J. B* **32** 49  
Vidhyadhiraja N S and Logan D E 2004 *Eur. Phys. J. B* **39** 313–334